MODIFIED ALGORITHM FOR MINERAL IDENTIFICATION IN LWIR HYPERSPECTRAL IMAGERY

Bardia Yousefi[1], Saeed Sojasi[1], Kévin Liaigre[2], Clemente Ibarra Castanedo[1], Georges Beaudoin[2], François Huot[2], Xavier P. V. Maldague[1], Martin Chamberland[3]

[1] Computer vision and systems laboratory, Laval University, 1065, av. de la Medicine, Quebec, City (Québec) G1V 0A6, Canada
[2] Department of Geology and Geological Engineering, Laval University, 1065, av. de la Medicine, Quebec City (Québec) G1V 0A6, Canada
[3] Telops, Inc., 100-2600 St-Jean-Baptiste Ave, Québec, Qc, G2E 6J5, Canada

PROJECT DESCRIPTION

The goal of this research lies on the clustering analysis for identification of the mineral grains in infrared thermal spectroscopy (LWIR 7.7-11.8µm wavelength range). Here, there are two different strategies investigated by modifying the clustering algorithm hierarchy before or after applying spectral comparison techniques. The proposed automatic identification algorithm strives to identify Biotite, Diopside, Epidote, Goethite, Kyanite, Scheelite, Smithsonite, Tourmaline, Quartz minerals grains.

EXPERIMENTAL SETUP

Experimental setup and hyperspectral image from mineral grains samples (as an example) are revealed in the figure. The experiment was conducted using an uniform heating source, an InfraGold plate, and a suitable macro lens that was especially designed for the use of the hyperspectral camera in laboratory conditions. Hyperspectral images with and without heating source and the arrangement of mineral grains are presented in the picture (lower-left side of the figure).

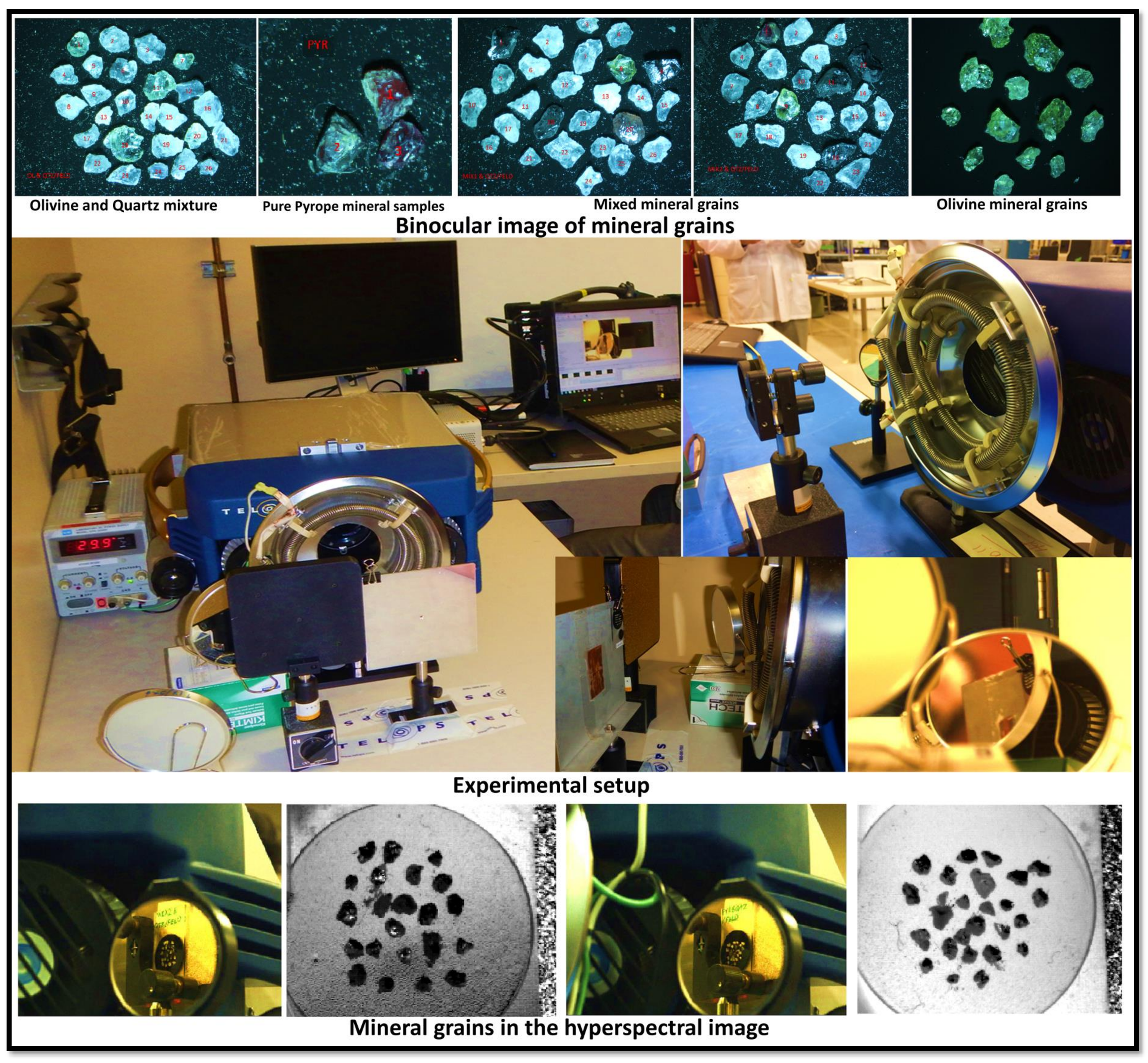

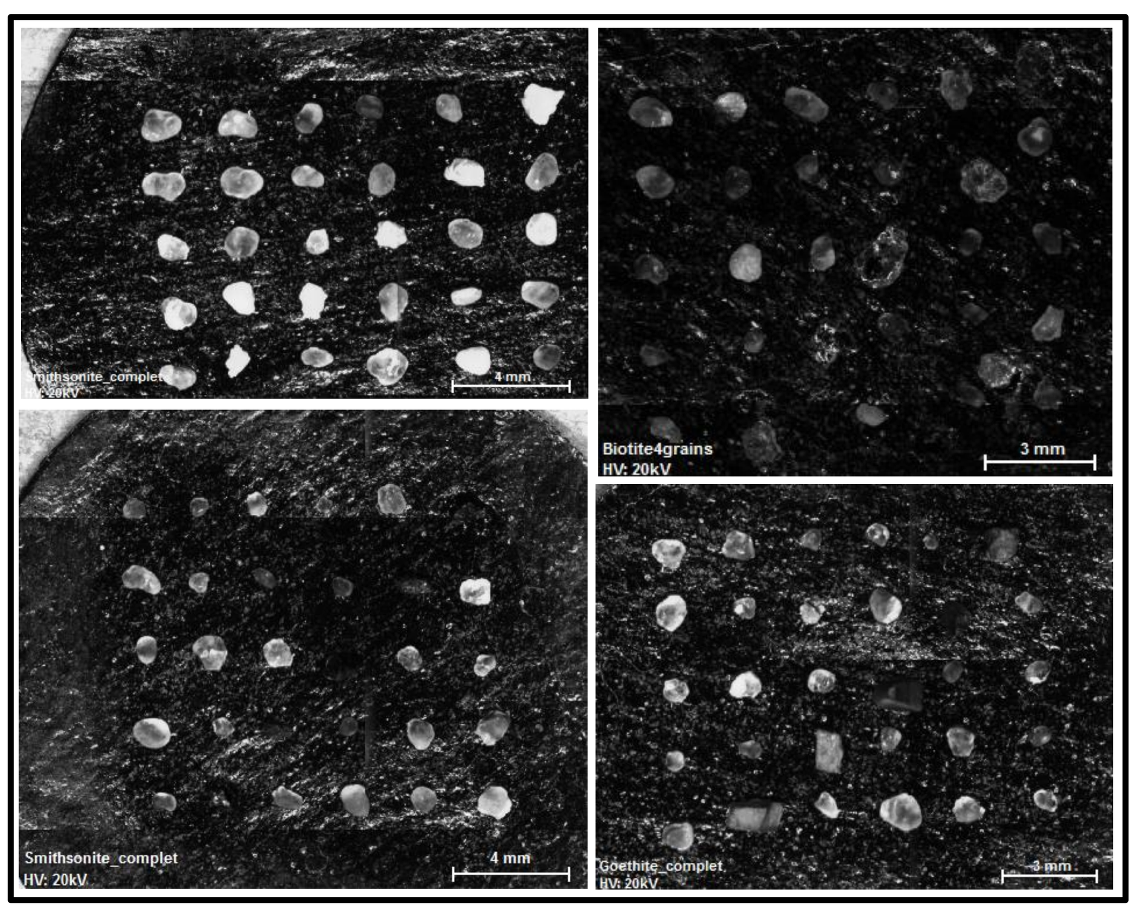

µXRF

The figure represents the images which were taken by Micro x-ray fluorescence (µXRF). µXRF can show the mineral contamination and tracking particular minerals among the samples. It provides a mapping corresponding to the minerals by having better accuracy and helps to create a Ground Truth (GT) for our analysis. Applying the GT considers as a vital step to compare the computational results to GT and finding the accuracy and reliability of the system.

Algorithm I	
Given	Input data $\boldsymbol{I(x,y,z)} \in \boldsymbol{R}^{N\times M\times Z}$ where $\boldsymbol{I(x,y)} \in \boldsymbol{R}^{N\times M}$ is the spatial dimension selected as the Region of Interest(RoI) and its unit is pixels, $\boldsymbol{z}$ is the spectral resolution and depends on hyperspectral camera and acquisition properties.
Step 1	Calculation of the reflectance of RoI $\boldsymbol{R}(\boldsymbol{x},\boldsymbol{y}) = \frac{I_{DW_{ON}}(x,y) - I_{DW_{OFF}}(x,y)}{\acute{I}_{IG_{ON}} - \acute{I}_{IG_{OFF}}}$. $\acute{\boldsymbol{I}}_{\boldsymbol{IG_{ON}}}, \acute{\boldsymbol{I}}_{\boldsymbol{IG_{OFF}}}$ are the radiance of the Infragold plate while the heating source is on and off, respectively (they are constant spectra). $\boldsymbol{I}_{\boldsymbol{DW_{ON}}}(\boldsymbol{x},\boldsymbol{y}), \boldsymbol{I}_{\boldsymbol{DW_{OFF}}}(\boldsymbol{x},\boldsymbol{y})$ are two spectral radiances where the heating source (down-welling radiation) is on and off in the $\boldsymbol{x},\boldsymbol{y}$ spatial position.
Step 2	Calculation of the spectral comparison techniques: $\mathbf{M}_{\boldsymbol{i}}(\boldsymbol{x},\boldsymbol{y}) = \boldsymbol{ST_j}(\boldsymbol{R}(\boldsymbol{x},\boldsymbol{y}), \boldsymbol{\Phi_i})$ $\boldsymbol{ST_j}$ represents the spectral techniques and j reveals the number of techniques exploited. $\boldsymbol{\Phi_i} \in \boldsymbol{R}^{\boldsymbol{z}}$ is the reference spectra (i.e. ASTER/JPL) and $\boldsymbol{i}$ is the number of spectra.
Step 3	False color generation ($\Psi_{\boldsymbol{RGB}}$), is dependent on $\boldsymbol{i}$ in $\boldsymbol{\Phi_i}$. For every targeted spectrum $(\boldsymbol{R},\boldsymbol{G},\boldsymbol{B})$, the amounts will change.
Output	Clustering $\Psi_{\boldsymbol{RGB}}$ to obtain the clusters where the identity of the mineral grains is revealed. The output will be $\boldsymbol{C_J}$. C shows the clusters and $\boldsymbol{J}$ represents cluster (J) which is related to the targeted mineral grains ($\boldsymbol{0} \le \boldsymbol{J} \le \boldsymbol{k}$, $\boldsymbol{k}$ is the total number of clusters).

Algorithm II	
Given	Input data $\boldsymbol{I(x,y,z)} \in \boldsymbol{R}^{N\times M\times Z}$ where $\boldsymbol{I(x,y)} \in \boldsymbol{R}^{N\times M}$ is the spatial dimension selected as the Region of Interest(RoI) and its unit is pixels, $\boldsymbol{z}$ is the spectral resolution and depends on the hyperspectral camera and acquisition properties.
Step 1	Calculation of the reflectance of RoI $\boldsymbol{R}(\boldsymbol{x},\boldsymbol{y}) = \frac{I_{DW_{ON}}(x,y) - I_{DW_{OFF}}(x,y)}{\acute{I}_{IG_{ON}} - \acute{I}_{IG_{OFF}}}$. $\acute{\boldsymbol{I}}_{\boldsymbol{IG_{ON}}}, \acute{\boldsymbol{I}}_{\boldsymbol{IG_{OFF}}}$ are the radiance of the Infragold plate while the heating source is on and off, respectively (they are constant spectra). $\boldsymbol{I}_{\boldsymbol{DW_{ON}}}(\boldsymbol{x},\boldsymbol{y}), \boldsymbol{I}_{\boldsymbol{DW_{OFF}}}(\boldsymbol{x},\boldsymbol{y})$ are two spectral radiances where the heating source (down-welling radiation) is on and off in the $\boldsymbol{x},\boldsymbol{y}$ spatial position.
Step 2	Clustering $\boldsymbol{I}_{(\boldsymbol{v},\boldsymbol{z})}$ into k categories shown by $\boldsymbol{C_k}$, $\boldsymbol{v} \in \boldsymbol{R}^{\boldsymbol{V}}$ is the spatial resolution in the vector form. The clustering is based on the spectral difference among the clusters ($\boldsymbol{0} \le \boldsymbol{J} \le \boldsymbol{k}$). $\dot{\boldsymbol{C}}_{\boldsymbol{k}}$ is the best representative of the cluster applying Non-Negative Matrix Factorization (NMF).
Step 3	Calculation of the spectral comparison techniques: $\mathbf{M}_{\boldsymbol{i}}(\boldsymbol{x},\boldsymbol{y}) = \boldsymbol{ST_j}(\dot{\boldsymbol{C}}^{\boldsymbol{s}}{}_{\boldsymbol{k}}, \boldsymbol{\Phi_i})$ $\boldsymbol{ST_j}$ is represents the spectral techniques and $\boldsymbol{j}$ reveals the number of techniques exploited (e.g. $\mathbf{j = 1 \rightarrow MAM_1 = NCC}$). s represents a sample from the cluster k. $\boldsymbol{\Phi_i} \in \boldsymbol{R}^{\boldsymbol{z}}$ illustrates the reference spectra (i.e. ASTER/JPL) and $\boldsymbol{i}$ is the number of spectra.
Output	False color generation ($\Psi_{\boldsymbol{RGB}}$), is dependent on $\boldsymbol{i}$ in $\boldsymbol{\Phi_i}$. For every targeted spectrum, the amount of $(\boldsymbol{R},\boldsymbol{G},\boldsymbol{B})$ will change. The output will be, $\Psi_{\boldsymbol{RGB}}$, an image where the materials have been marked by different color.

Two proposed algorithms are shown for Clustering of spectral comparison (**Algorithm I**) and The likelihood of the Spectral clusters (**Algorithm II**), for automatic identification of the mineral grains. In the both algorithms Spectral Angel Mapper (SAM) and Normalized Cross Correlation(NCC) are employed as the spectral comparison techniques.

RESULTS

The results of SAM and NCC for Biotite, Diopside, Epidote, Geothite, Kynite, Scheelite, Smithsonite, and Tourmaline are shown applying the first algorithm. The arrangement of the mineral grains is also shown. The minerals are represented in the false colors to better reveal the mineral grains.

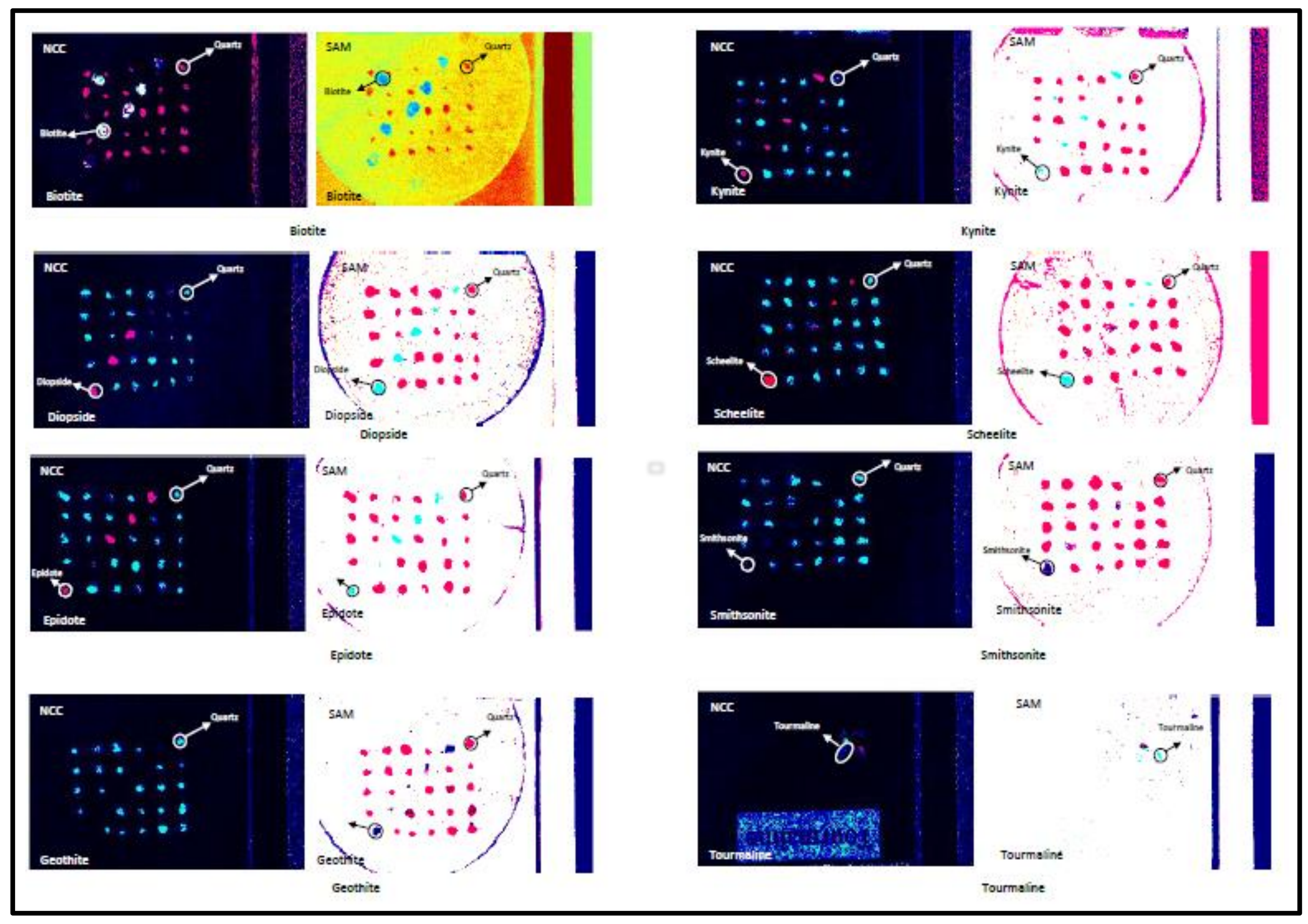

Figure below depicts the results of clustering for the second algorithm. In the second algorithm, the spectra directly clustered and the best representative of each group compare to the ASTER spectral library. Afterward, the false colors generate correspond to the amount of the spectral difference. The figure shows the final false color results and representative of the groups and ASTER spectrum equivalent to the mineral.

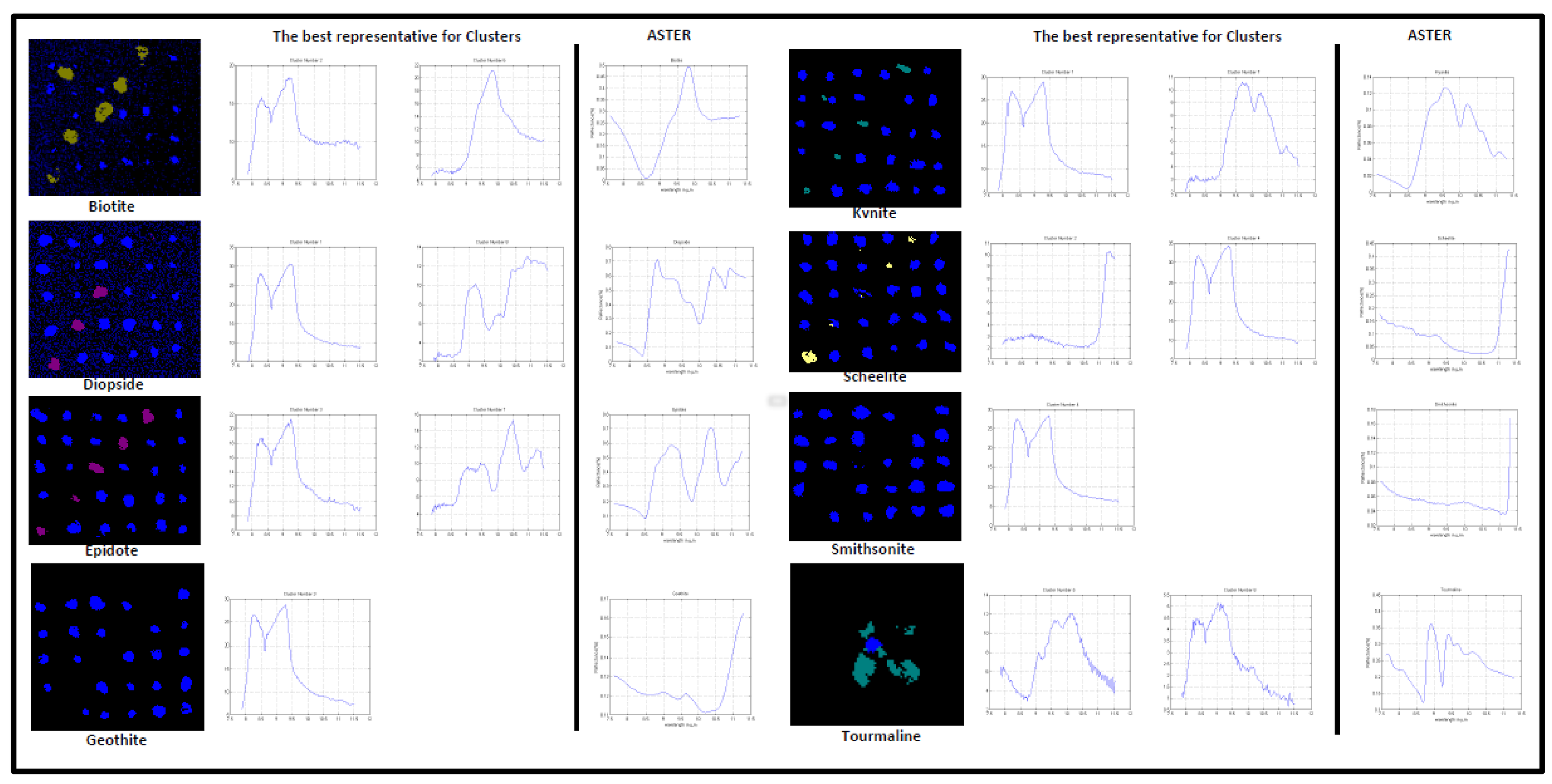

SUMMARY

The application of hyperspectral infrared imagery in the different fields of research is significant. It is mainly used in remote sensing for target detection, vegetation detection, urban area categorization, astronomy and geological applications. The geological applications of this technology mainly consist in mineral identification using airborne or satellite imagery. We address a quantitative and qualitative assessment of mineral identification in the laboratory condition. We strive to identify nine different mineral grains (Biotite, Diopside, Epidote, Goethite, Kyanite, Scheelite, Smithsonite, Tourmaline, Quartz). A hyperspectral camera in the Long Wave Infrared (LWIR, 7.7-11.8 µm) with a LW-marco lens having spatial resolution of 100µm, an infragold plate, and a heating source are the instruments used in the experiment. This paper addresses a quantitative and qualitative assessment on an algorithm for identification of minerals in the laboratory (indoor) conditions. The algorithm clusters all the pixel-spectra to identify the minerals. Then the best representatives of each cluster are chosen and compared with the spectral library of JPL/NASA through spectral comparison techniques. Techniques give the comparison amount as features which converts into false colors as the results of this algorithm. Spectral techniques used are Adaptive Matched Subspace Detector (AMSD) algorithm, PCA Local Matched Filter (PLMF), Spectral angle mapper (SAM), and Normalized Cross Correlation (NCC). Nine different mineral grains were tested in the Long Wave Infrared (LWIR, 7.7-11.8 µm). The results of the algorithm indicate significant computational efficiency (more than 20 times faster than previous approach) and promising performance for mineral identification.

References

[1] Baldridge, A. M., Hook, S. J., Grove, C. I., & Rivera, G. (2009). The ASTER spectral library version 2.0. Remote Sensing of Environment, 113(4), 711-715.
[2] Yousefi, B., Sojasi, S., Castanedo, C. I., Beaudoin, G., Huot, F., Maldague, X. P., ... & Lalonde, E. (2016, May). Emissivity retrieval from indoor hyperspectral imaging of mineral grains. In SPIE Commercial+ Scientific Sensing and Imaging (pp. 98611C-98611C). International Society for Optics and Photonics.
[3] MacQueen, J. (1967, June). Some methods for classification and analysis of multivariate observations. In *Proceedings of the fifth Berkeley symposium on mathematical statistics and probability* (Vol. 1, No. 14, pp. 281-297).
[4] Baldridge, A. M., Hook, S. J., Grove, C. I., & Rivera, G. (2009). The ASTER spectral library version 2.0. Remote Sensing of Environment, 113(4), 711-715.
[5]Rivard, B., Feng, J., Huot, F., & Chamberland, M. FIRST GEOLOGICAL CASE STUDY OF THE AIRBORNE LONGWAVE HYPERSPECTRAL HYPER-CAM SYSTEM, THETFORD MINES, QUEBEC.

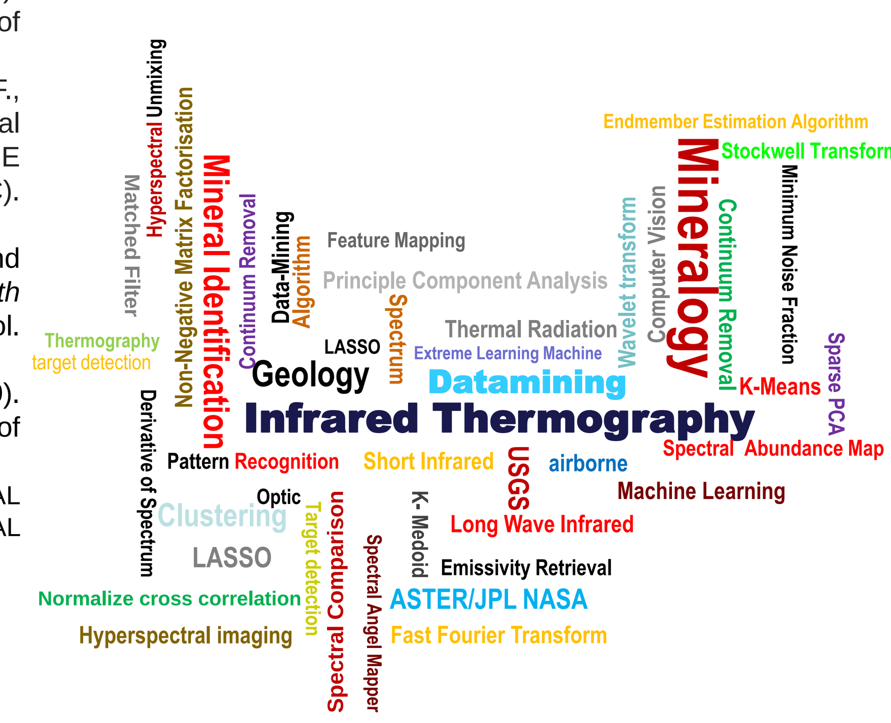

We thank FRQ-NT (Fonds de Recherche du Québec – Nature et Technologies) for their financial support.